J Supercond Nov Magn (2012) 25:779–784
DOI 10.1007/s10948-011-1338-7

ORIGINAL PAPER

Flux-Line-Lattice Melting and Upper Critical Field of $Bi_{1.65}Pb_{0.35}Sr_2Ca_2Cu_3O_{10+\delta}$ Ceramic Samples

E. Govea-Alcaide · P. Muné · R.F. Jardim

Received: 14 September 2011 / Accepted: 3 October 2011 / Published online: 28 October 2011

Abstract We have conducted magnetoresistance measurements $\rho(T, H)$ in applied magnetic fields up to 18 T in $Bi_{1.65}Pb_{0.35}Sr_2Ca_2Cu_3O_{10+\delta}$ ceramic samples which were subjected to different uniaxial compacting pressures. The anisotropic upper critical fields $H_{c2}(T)$ were extracted from the $\rho(T, H)$ data, yielding $H_{c2}^{ab}(0) \sim 130$ T and the out-of-plane superconducting coherence length $\xi^c(0) \sim 3$ Å. We have also estimated $H_{c2}^{c}(0) \sim 4.4$ T and $\xi^{ab}(0) \sim 90$ Å. In addition to this, a flux-line-lattice (FLL) melting temperature T_m has been identified as a second peak in the derivative of the magnetoresistance $d\rho/dT$ data close to the superconducting transition temperature. An H_m vs. T phase diagram was constructed and the FLL boundary lines were found to obey a temperature dependence $H_m \propto (T_c/T - 1)^{\alpha}$, where $\alpha \sim 2$ for the sample subjected to the higher compacting pressure. A reasonable value of the Lindemann parameter $c_L \sim 0.29$ has been found for all samples studied.

Keywords Bi-based superconductors · Weak links · Electrical conductivity

1 Introduction

One of the most important features of high-T_c superconductors is the high degree of anisotropy of both normal and superconducting properties due to their layered crystal structure. The evaluation of the anisotropy of these low-dimensional materials can be inferred by measurements of their anisotropic quantities as the electrical resistivity, ρ, the upper critical field, H_{c2}, the critical current density, J_c, etc. [1]. In addition, other features of these compounds as the large London penetration depth, high superconducting critical temperatures, and disorder conspire for strong fluctuations of the vortices that can lead to the melting of the vortex lattice. This is responsible for a new boundary line in the H vs. T phase diagram above the lower critical field line, $H_{c1}(T)$. This new boundary line, commonly termed as the irreversibility line or the flux-line-lattice melting line (FLL), separates a magnetically irreversible and zero-resistance state from a reversible state with dissipative electrical transport properties [2].

The anisotropic behavior of high-T_c materials have been frequently studied via H vs. T phase diagram, and the boundaries lines have been determined in single crystal specimens [1–4]. On the other hand, similar determinations, when using polycrystalline samples, would take into account several approximations arising from the complex granular nature of ceramic samples which contain voids, cracks, grain boundaries, and orientational disorder of the grains [5]. The features of ceramic samples also play an important role in limiting transport current in polycrystalline specimens of high-T_c superconductors. Besides this, it is well known that very low values of the superconducting critical current in polycrystalline samples are mainly due to the misorientation between grains. Within this context, high angle grain boundaries act as Josephson coupled weak links, leading to a significant field-dependent suppression of the supercurrent tunneling across grain boundaries [6].

As mentioned above, a simple way to study both the anisotropic behavior and the boundary lines belonging to the

E. Govea-Alcaide (✉) · P. Muné
Departamento de Física, Universidad de Oriente, Patricio Lumumba s/n, P.O. Box 90500, Santiago de Cuba, Cuba
e-mail: malvareza@udg.co.cu

R.F. Jardim
Instituto de Física, Universidade de São Paulo, CP 66318, 05315-970, São Paulo, SP, Brazil

H vs. T phase diagram in high-T_c superconductors is performing temperature and magnetic field dependence of the electrical resistivity $\rho(T, H)$. In the $\rho(T, H)$ data, the broadening of the superconducting transition in applied magnetic fields $H > H_{c1}$ has been extensively investigated in several cuprates [1, 3, 4, 7–14]. There is a consensus that the width of the superconducting transition is strongly influenced by the anisotropy associated with the orientation of the applied magnetic field with respect to the CuO_2 planes [3, 15, 16].

In this work we have performed a systematic study of the transport properties in $Bi_{1.65}Pb_{0.35}Sr_2Ca_2Cu_3O_{10+\delta}$ ceramic samples which were subjected to different uniaxial compacting pressures. We first mention that in a previous study, transport measurements performed in the same samples revealed an improvement of both normal and superconducting properties [17]. Thus, measurements of the temperature dependence of the electrical resistivity under applied magnetic fields up to 18 T have enabled us to discuss other features of these anisotropic compounds. X-ray diffraction (XRD), taken on both powder and bulk samples, has been performed as a complementary characterization. The main contribution of this paper is related to the influence of the uniaxial compacting pressure on the H vs. T phase diagram of (Bi-Pb)-2223 compounds. The quantitative analysis carried out suggests that increasing compacting pressure results in an increase of the texture degree of the samples. We have used these textured samples of the (Bi-Pb)-2223 compound to estimate important superconducting parameters such as the upper critical fields and the superconducting coherence lengths.

2 Experimental procedure

Polycrystalline samples of $Bi_{1.65}Pb_{0.35}Sr_2Ca_2$ $Cu_3O_{10+\delta}$ (Bi-2223) were prepared from powders of Bi_2O_3, PbO, $SrCO_3$, $CaCO_3$, and CuO, which were mixed in an atomic ratio of Pb:Bi:Sr:Ca:Cu (0.35:1.65:2:2:3). Details of the sample preparation process are given elsewhere [18]. Before the last heat treatment, the powders were uniaxially pressed at ∼98 MPa, referred to as **Sample P1**, and ∼588 MPa, referred to as **Sample P6**. The typical dimensions of the pellets were $d = 10$ mm in diameter and $h = 1$ mm in height. The last heat treatment of the pellets was performed in air at 845 °C for 40 h followed by slow cooling. The phase identification in both powder and bulk samples has been made by means of X-ray diffractometry. The X-ray patterns were obtained in a Bruker-AXS D8 Advance diffractometer and the evaluation of the degree of texture of the pellet samples was made by using the same technique. These measurements were performed at room temperature using Cu Kα radiation in the $3° \leq 2\theta \leq 80°$ range with a 0.02° (2θ) step size, and 5 s counting time.

The temperature dependence of the electrical resistivity, $\rho(T)$, in the temperature range $2 \leq T \leq 300$ K and in applied magnetic fields, H, ranging from 0 to 18 T were performed by using a commercial Linear Research (Model LR-700) ac resistance bridge operating at a frequency of 16 Hz. For these measurements, copper electrical leads were attached to Ag film contact pads on parallelepiped-shaped samples using Ag epoxy. The typical dimensions of the samples were $t = 1$ mm (thickness), $w = 2$ mm (width), and $l = 10$ mm (length). The magnetic field H was always applied perpendicularly to both the thickness of the samples and to the excitation current, I, that has been injected along the major length of samples. We have estimated the remanent field of the superconducting magnet of 0.03 T. The excitation currents used in these experiments were typically of 1 mA ($J \sim 0.5$ A/cm^2).

3 Results and discussion

The X-ray diffraction patterns, taken on bulk samples, indicated that all samples have similar chemical composition and their indexed reflections are related to the high-T_c Bi-2223 phase [17, 18]. The unit-cell parameters were calculated regarding an orthorhombic unit cell and the obtained values $a = 5.410$ Å, $b = 5.413$ Å, and $c = 37.152$ Å are in line with those reported elsewhere for the same compound [19]. The values of a, b, and c were found to be similar for all samples subjected to different compacting pressures. Also, the data show that the height of the peak (00$\underline{10}$) increases monotonically with increasing compacting pressure suggesting that higher compacting pressures improved the texture of the samples, resulting in a better alignment of the grains. The grains of the sample **P6** are aligned preferentially with their c-axes parallel to the compacting direction.

The $\rho(T)$ curves for samples **P1** (see Fig. 1(a)) and **P6** (see Fig. 1(b)) under the influence of applied magnetic fields ranging from 0 to 18 T are displayed in Fig. 1. Increasing magnetic field results in appreciable changes in the shape of the $\rho(T, H)$ curves in the superconducting state. As the magnetic field increases, the superconducting transition becomes broader. We have found that all curves exhibit a transition to the superconducting state below the so-called onset superconducting critical temperature $T_{on} \sim 120$ K. Besides, the temperature in which the zero-resistance state is observed, the offset temperature T_{off}, decreases abruptly with increasing H. It was also found that T_{off} decreases from 95.6 K to 32.5 K in sample **P1** when the applied magnetic field is varied from 0 to 18 T. For the same magnetic field window, T_{off} was found to decrease from 97.7 K to 35.2 K in sample **P6**. We want to point out that the observed values of T_{off} at $H = 0$ T are slightly lower when compared with the previous result of ∼102 K in Bi-2223 materials [17, 18,

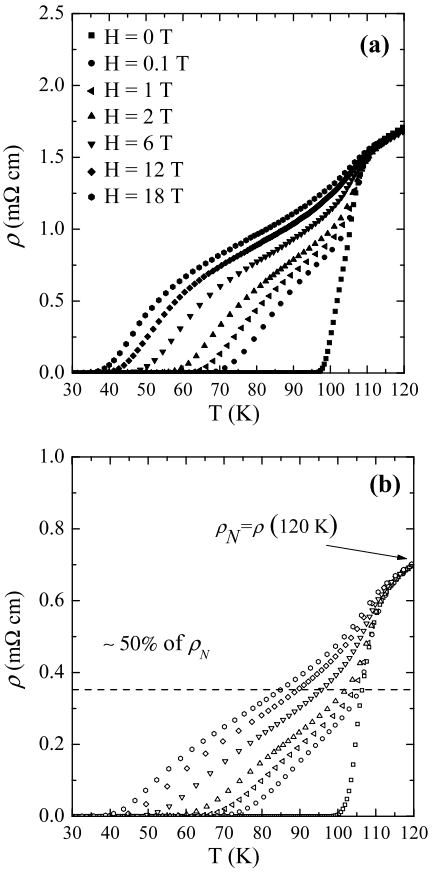

Fig. 1 Resistive transition in applied magnetic fields up to 18 T of samples **P1** (**a**) and **P6** (**b**). Values of the upper critical field H_{c2} were obtained from the 50% drop in $\rho(T, H)$ curves across the superconducting transition

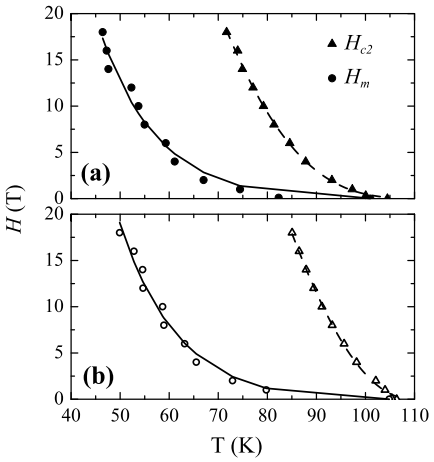

Fig. 2 An H vs. T/T_c phase diagram for samples **P1** (**a**) and **P6** (**b**). The dashed line in H_{c2} data corresponds to a fit to the phenomenological GL relation (see (1)). The FLL melting curves, H_m vs. T, were fitted by using (4). In this case, the fitting curves are displayed in solid lines

Table 1 Relevant parameters extracted from fitting the H_{c2} vs. T curves to (1)

Sample	$H_{c2}^{ab}(0)$ (T)	$H_{c2}^{c}(0)$ (T)	$\xi_{ab}(0)$ (Å)	$\xi_c(0)$ (Å)	T_c (K)	α
P1	122	3.9	91	3.0	105.5	3.7
P6	136	4.4	87	2.8	107	2.2

20]. This is a consequence of the remanent magnetic field of the superconducting magnet.

The electrical resistivity data are useful to construct an H_{c2} vs. T phase diagram for each sample [1, 21]. The (H, T) pairs were extracted from the 50% falls in the electrical resistivity curves at the superconducting transition (see Fig. 1(b)). As shown in Fig. 2, the $H_{c2}(T)$ curves of samples **P1** and **P6** are qualitatively similar. Notice that $H_{c2}(T)$ curves exhibit an upward curvature near T_c, typical of other cuprates, but rather different from the linear behavior of $H_{c2}(T)$ derived from both Ginzburg–Landau and BCS theories.

We start our discussion by estimating the value of the critical field at zero temperature, $H_{c2}(0)$, by using a fitting all the (H, T) pairs to the Ginzburg–Landau relation [23]:

$$H_{c2}(T) = H_{c2}(0)\left[1 - (T/T_c)^2\right]^{\alpha} \tag{1}$$

where $T_c = (T_{\text{on}} + T_{\text{off}})/2$ has been used for the superconducting critical temperature, and α is an exponent.

We have assumed that due to the combination of the high anisotropy of the system and the misorientation of the superconducting grains, the estimate value of H_{c2} at zero temperature would reflect the upper critical field along the ab-plane $H_{c2}^{ab}(0)$ of the anisotropic material. Also, estimated values of $H_{c2}^{c}(0)$ were obtained by using an anisotropic ratio $\gamma = H_{c2}^{ab}(0)/H_{c2}^{c}(0) \sim 31$, as reported for Bi-2223 whiskers [1].

Table 1 displays the obtained values of $H_{c2}(0)$, T_c, and α. It is worth mentioning that the values of $H_{c2}(0)$, ~ 130 T along the ab-plane, are smaller than those reported for Bi-2223 whiskers [1] ($H_{c2}^{ab}(0) = 1210$ T and $H_{c2}^{c}(0) = 32$ T) and Ag/Bi-2223 tapes [24] ($H_{c2}^{ab}(0) = 830$ T). However, the obtained values are in the range 45–200 T, as previously reported in melt-quenched $Bi_{1.6}Pb_{0.3}Te_{0.1}Sr_2Ca_3Cu_4O_y$ samples [25].

The influence of the grain misalignment on the $H_{c2}(T)$ boundary line is revealed by analyzing the values of the exponent α (see (1)). The latter was found to decrease from 3.7 ± 0.7 to 2.2 ± 0.2, indicating that α decreases appreciably with increasing compacting pressure, or more appropriately, with a better alignment of grains along the ab plane. We also mention that values of α in the range 1.5 to 2.0 are frequently observed in single-crystals specimens of high-T_c materials, a result that clearly lends credence to our analysis [23].

From in-plane and out-of-plane values of the orbital critical field, we were able to estimate both the in-plane, $\xi_{ab}(0)$,

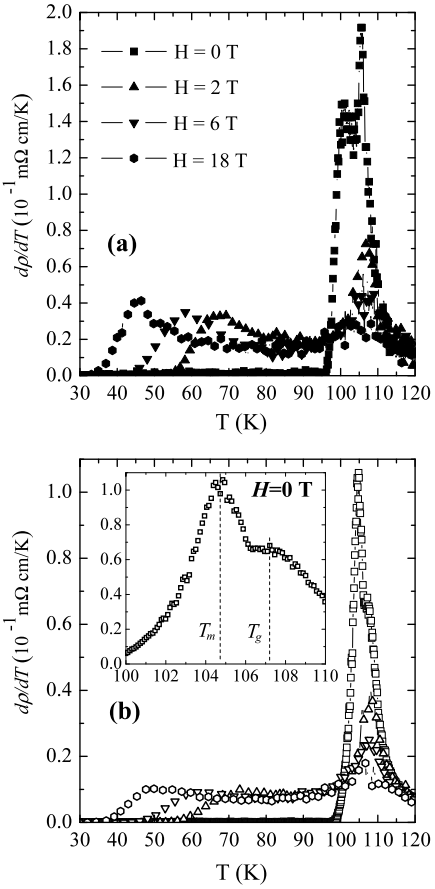

Fig. 3 Derivative $d\rho/dT$ of the electrical resistivity curves (see Fig. 1) of samples **P1** (**a**) and **P6** (**b**). The *inset* displays an expanded view of the curve at $H = 0$ T belonging to the sample **P6** in (**b**). The FLL melting transition temperature, T_m, is identify as the second peak in the derivative data, as discussed in the text

and the out-of-plane, $\xi_c(0)$, coherence lengths by using the Ginzburg–Landau relations:

$$\xi_{ab}^2(0) = \frac{\Phi_0}{2\pi H_{c2}^c(0)} \tag{2}$$

and

$$\xi_c(0) = \frac{\Phi_0}{2\pi H_{c2}^{ab}(0)\xi_{ab}(0)} \tag{3}$$

where Φ_0 is the flux quantum. The obtained values are listed in the Table 1. It should be noted that $\xi_{ab}(0) \gg a$ and $\xi_c(0) \ll c$, where $a \approx b$ and c are the unit-cell parameters, as usually seen in these high anisotropic cuprates.

The derivative curves of the electrical resistivity, $d\rho/dT$, at fixed applied magnetic fields for samples **P1** and **P6**, are displayed in Figs. 3(a) and 3(b). The common feature of the curves is the occurrence of two well defined peaks which are characterized by a height, or intensity, and a position in temperature. Let us consider as a reference the $\rho(T)$ data taken at $H = 0$ T on the sample **P6** (see the inset of Fig. 3(b)) where two peaks at $T_g \approx 106.5$ K and $T_m \approx 104.8$ K are clearly identified. Five general conclusions can be drawn from the data shown in Fig. 3: (a) $T_m \leq T_g$ in all curves; (b) the position of T_g is essentially magnetic field independent for both samples; (c) the height of the $d\rho/dT$ peak at $T = T_g$ decreases appreciably with increasing magnetic field. Such a decrease was found to reach ∼75 and 80% in samples **P1** and **P6**, respectively, when H is varied from zero to 18 T; (d) the height of the $d\rho/dT$ peak at $T = T_m$ is much more sensitive to the applied magnetic field and decreases ∼25 and 11% in samples **P1** and **P6**, respectively; and (e) between $H = 0$ and 18 T the position of T_m decreases ∼52% in both samples: in the sample **P1**, the value of T_m drops from ∼101 to ∼47 K, while in sample **P6** it is between ∼105 and ∼50 K.

The behavior of $\rho(T, H)$ in the vicinity of T_m indicates that the intergranular properties have been improved with increasing compacting pressure. This is certainly caused by the improvement of the degree of texture which in turn has enhanced the grain connectivity [17, 20, 26]. The latter is crucial for the establishment of Josephson coupling between grains at temperatures below T_m. A fingerprint of this behavior is the difference between the height of the $d\rho/dT$ peak at $T = T_m$. Moreover, such a change in the coupling between grains can also be inferred from the occurrence of the double resistive superconducting transition displayed in Fig. 1, a feature much more pronounced in sample **P1** [27–29].

The occurrence of two well defined peaks in $d\rho/dT$ curves close to the superconducting transition temperature is usually related to the intra- and intergranular superconducting transitions [27–30]. However, we first mention that the height of the peaks in our curves remains essentially unaltered when the applied magnetic field is increased. Such a behavior differs from those reported in other polycrystalline samples where the height of the second peak in $d\rho/dT$ curves decreases abruptly at relatively low (≤1 T) applied magnetic fields [31]. Under this circumstance, we assume that the peak in $d\rho/dT$ curves at $T = T_m$ is related to the flux-line-lattice melting or the irreversibility line at the intragranular level [3, 4]. Within this context, Fig. 2 displays the magnetic field phase diagram, H_m vs. T, for samples **P1** and **P6**. As has been proposed for BSCCO materials [2, 32], the FLL boundary line can be fitted by using the relationship:

$$H_m(T) = A(T_c/T - 1)^2, \tag{4}$$

where

$$A = \frac{\Phi_0^5 c_L^4}{16\pi^3 \lambda_{ab}^4(0)\mu_0^2\gamma^2 k_B^2 T_c^2} \tag{5}$$

c_L is the Lindemann parameter, λ_{ab} is the in-plane London penetration depth, μ_0 is the magnetic permeability of vacuum, and k_B is the Boltzmann constant. The best fit is obtained for $A = 10 \pm 0.4$ T, by using $T_c = 105.5$ K, for sample **P1** and $A = 14 \pm 0.4$ T ($T_c = 107$ K) for sample **P6**.

By using (2), (3), and (4) and solving (5) for c_L^4, one obtains [22]:

$$c_L^4 \approx \frac{2\pi^3 \mu_0^2 k_B^2 \gamma^3 \lambda_{ab}^4(0) T_m^2}{\Phi_0^4 \xi_{ab}^2(0)} \frac{H_m}{H_{c2}^{ab}(0)}. \quad (6)$$

Assuming $\lambda_{ab}(0) = 1240$ Å [32], and $\gamma = 31$ [1, 32], a value of the Lindemann parameter $c_L = 0.29$ is obtained for both samples. The other parameters in (6) were $H_m = 18$ T, $T_m = 46.4(49)$ K, $T_c = 105.5(107)$ K, $H_{c2}^{ab}(0) = 122(136)$ T, and $\xi_{ab}(0) = 91(87)$ Å, as displayed in Table1 for samples **P1** and **P6**, respectively. It is important to mention that the value of $c_L = 0.29$ is within the range expected for high-T_c materials, i.e., from 0.1 to 0.5 [33]. Indeed, such a value of c_L is in excellent agreement with $c_L = 0.28$ calculated in c-axis oriented bulk Bi-2223 compounds [32].

Based on the estimated value of $c_L = 0.29$ we are leading to conclude that changes in the texture degree of the samples resulted in small variations in the H_m vs. T boundary line. This also implies that tilting the magnetic field would result in little changes on the thermodynamics of the vortex state. Such a result seems unexpected at first glance but can be interpreted when similar data obtained in single-crystals of $YBa_2Cu_3O_{7-\delta}$ are considered [4]. The authors of Ref. [4] have observed changes in the H_m vs. T boundary line as a function of the magnetic field orientation with respect to the Cu–O_2 planes. The results indicated that such changes were perceived only for magnetic fields applied to angles higher than 40°. In addition to this, we also argue that recent magneto-optical measurements and molecular dynamics simulations in $Bi_2Sr_2CaCu_2O_8$ with columnar defects give support to our estimates of c_L [34]. It was found that the dynamics properties of porous vortex matter are very sensitive to the angle between the applied magnetic field and the columnar defects. On the other hand, the thermodynamic melting were found to be angle independent. As far as our samples are concerned, a rather small difference in the orientation of their grains along the c direction is expected. In order to support this statement, the degree of texture of our samples must be considered. Within the framework of the current conduction model proposed by Díaz et al. [5], the degree of texture of a polycrystalline sample is represented by the misalignment factor f. Previous estimates of f in our samples resulted in values close to 0.6 and 0.7 for samples **P1** and **P6**, respectively [17, 26]. Such a little increase in the magnitude of f with increasing compacting pressure agrees well with the small changes observed in the $H_m(T)$ line of our two samples.

4 Conclusions

In summary, we have presented here the magnetic phase diagram of $(Bi\text{-}Pb)_2Sr_2Ca_2Cu_3O_{10+\delta}$ ceramic samples which were subjected to different uniaxial compacting pressures. The $H_{c2}(0)$ vs. T and H_m vs. T boundary lines have been extracted from electrical resistivity measurements in applied magnetic fields up to 18 T. We have found that the temperature dependence of H_{c2} is much more sensitive to the degree of texture of the samples, as inferred from the ∼ 40 % decrease of the exponent α with increasing compacting pressure. We have also estimated the upper critical field $H_{c2}^{ab}(0) \sim 130$ T and the coherence length along the Cu–O planes $\xi^{ab}(0) \sim 90$ Å, provided that the anisotropy of the system is assumed to be $\gamma = 31$. The out-of-plane parameters were $H_{c2}^{c}(0) \sim 4.4$ T and $\xi^{c}(0) \sim 3$ Å. From the second peak of the derivative of $\rho(T, H)$ curves we were able to discuss the flux-line lattice melting transition of the samples. We have found no appreciable differences in the H_m vs. T boundary lines between both samples. The Lindemann parameter $c_L \sim 0.29$ was found to be compacting pressure independent and is in line with others found in layered cuprates.

Acknowledgements This work was supported by the Brazil agencies Fundação de Amparo à Pesquisa do Estado de São Paulo (FAPESP), Conselho Nacional de Desenvolvimento Científico e Tecnológico (CNPq), and Coordenação de Aperfeiçoamento de Pessoal de Nível Superior (CAPES). One of us E.G-A. acknowledges FAPESP under Grant No. 2010/52545-2. R.F.J. is CNPq fellow under Grant No. 304112/2010-0.

References

1. Matsubara, I., Tanigawa, H., Ogura, T., Yamashita, H., Kinoshita, M., Kawai, T.: Phys. Rev. B **45**, 7414 (1992)
2. Schilling, A., Jin, R., Guo, J.D., Ott, H.R.: Phys. Rev. Lett. **71**, 1899 (1993)
3. Charalambous, M., Chaussy, J., Lejay, P.: Phys. Rev. B **45**, 5091 (1992)
4. Kwok, W.K., Fleshler, S., Welp, U., Vinokur, V.M., Downey, J., Crabtree, G.W.: Phys. Rev. Lett. **69**, 3370 (1992)
5. Díaz, A., Maza, J., Vidal, F.: Phys. Rev. B **55**, 1209 (1997)
6. Hilgenkamp, H., Mannhart, J.: Rev. Mod. Phys. **74**, 485 (2002)
7. Tinkham, M.: Phys. Rev. Lett. **61**, 1658 (1988)
8. Palstra, T.T., Batlogg, B., van Dover, R.B., Scheemeyer, L.F., Waszczak, J.V.: Appl. Phys. Lett. **54**, 763 (1989)
9. Burlachkov, L., Mogilko, E., Schlesinger, Y., Strelniker, Y.M., Havlin, S.: Phys. Rev. B **67**, 104509 (2003)
10. Bhalla, G.L., Pratima, Amita Malik, Singh, K.K.: Physica C **391**, 17 (2003)
11. Ambegaokar, V., Halperin, B.I.: Phys. Rev. Lett. **22**, 1364 (1969)
12. Kosterlitz, J.M., Thouless, D.J.: J. Phys. C **6**, 1181 (1973)
13. Müller, K.A., Takashige, M., Bednorz, J.G.: Phys. Rev. Lett. **58**, 1143 (1987)
14. Kim, D.H., Gray, K.F., Kampwirth, R.T., Mckay, D.M.: Phys. Rev. B **42**, 6249 (1990)
15. Xu, X.J., Fu, L., Wang, L.B., Zhang, Y.H., Fang, J., Cao, X.W., Li, K.B., Hisashi, S.: Phys. Rev. B **59**, 608 (1999)
16. Salem, A., Jakob, G., Adrian, H.: Physica C **402**, 354 (2004)
17. Govea-Alcaide, E., Jardim, R.F., Muné, P.: Physica C **423**, 152 (2005)
18. Muné, P., Govea-Alcaide, E., Jardim, R.F.: Physica C **384**, 491 (2003)

19. Pandey, D., Mahesh, R., Singh, A.K., Tiwari, V.S.: Physica C **184**, 135 (1991)
20. Govea-Alcaide, E., Jardim, R.F., Muné, P.: Phys. Status Solidi A **202**, 2484 (2005)
21. Escote, M.T., Meza, V.A., Jardim, R.F., Ben-Dor, L., Torikachvili, M.S., Lacerda, A.H.: Phys. Rev. B **66**, 144503 (2002)
22. Tinkham, M.: Introduction to Superconductivity. McGraw-Hill, New York (1975)
23. Cyrot, M., Pavuna, D. (eds.): Introduction to Superconductivity and High-T_c Materials. World Scientific, Singapore (1992)
24. Chen, W.M., Wang, F., Jiang, S.S., Liu, H.K., Dou, S.X.: J. Supercond. **14**, 465 (2001)
25. Vlakhova, E.S., Nenkovb, K.A., Ciszekc, M., Zaleskic, A., Dimitrievd, Y.B.: Physica C **225**, 149 (1994)
26. Govea-Alcaide, E., Muné, P., Jardim, R.F.: Braz. J. Phys. **35**, 680 (2005)
27. Jardim, R.F., Ben-Dor, L., Stroud, D., Maple, M.B.: Phys. Rev. B **50**, 10080 (1994)
28. Jardim, R.F., de Andrade, M.C., Early, E.A., Maple, M.B., Stroud, D.: Physica C **232**, 145 (1994)
29. Jardim, R.F., Early, E.A., Maple, M.B.: J. Alloys Compd. **221**, 1 (1995)
30. Govea-Alcaide, E., García-Fornaris, I., Jardim, R.F., Muné, P.: Eur. Phys. J. B **58**, 373 (2007)
31. Viera, V.N., da Silva, J.P., Schaf, J.: Phys. Rev. B **64**, 094516 (2001)
32. Kopelevich, Y., Moehlecke, S., Torres, J.H.S.: Phys. Rev. B **49**, 1495 (1994)
33. Ryu, S., Doniach, S., Deutsher, G., Kapitulnik, A.: Phys. Rev. Lett. **68**, 710 (1992)
34. Avraham, N., Goldschmidt, Y.Y., Liu, J.T., Myasoedov, Y., Rappaport, M., Zeldov, E., van der Beek, C.J., Konczykowski, K., Tamegai, T.: Phys. Rev. Lett. **99**, 087001 (2007)